Tuning resonant optical transmission of metallic nanoslit arrays with embedded microcavities

Zhijun Sun* and Xiaoliu Zuo

Department of Physics, Xiamen University, Xiamen 361005, China
**Corresponding author: sunzj@xmu.edu.cn*

Received November 26, 2008; revised February 24, 2009; accepted March 20, 2009;
posted April 2, 2009 (Doc. ID 104525); published April 24, 2009

We numerically study the characteristics of optical transmission of metallic nanoslit arrays (MNSAs) with embedded microcavities (MC-MNSAs) and demonstrate that passbands of the transmission spectra can be monotonously tuned by adjusting the dimensions of the microcavities. The study discloses that spectra of conventional MNSAs and MC-MNSAs are determined mainly by cavity resonances of the slits or embedded microcavities, modified by in-plane surface-plasmon wave resonances. It is also found that coupling of cavity resonances between neighboring slits or microcavities has considerable effects on the passbands. The MC-MNSA structure is shown to have potentials in applications of tunable filter arrays. © 2009 Optical Society of America

OCIS codes: 260.3910, 240.6680, 260.5740, 120.2440.

Optical transmission of metallic nanoslit arrays (MNSAs) has been extensively studied over the past decade [1–7]. Besides complex physics of research interest, the structure is promising in many applications, e.g., for tunable filter arrays [8]. The main passbands of MNSAs are dependent on the structure dimensions (metal thickness, period, and slit width) for a given materials system. For filter arrays, the period is usually considered as the primary factor for passband tuning in design [8]. But recently we found that positions of the main transmission passbands of MNSAs are not monotonously dependent on the structural periods as thought [9], though this presently lacks experimental fact. The reason has been explained in [9], and the consistency in principles is also shown in this Letter for the proposed structure of metallic nanoslit arrays with embedded microcavities (MC-MNSAs).

The MC-MNSA structure consists of a conventional MNSA structure and microcavities embedded in each slit, which is schematically shown in Fig. 1(a). The channeling resonances in transmission are thus localized in the microcavities instead of simple slits. Transmission passbands can then be monotonously tuned in a wider range, as variation ranges of the microcavities' dimensions are enlarged. Besides, thoughtful design of this structure ensures such effects taking place in principle, which are all essential to form a transmission spectrum with a dominant passband: (i) in-plane surface plasmon (SP) resonance at the discontinuous metal-dielectric (or air) interfaces, achieved by keeping the slits very narrow near the entrances/exits; (ii) cavity resonance in the microcavities, which replaces the Fabry–Perot-like resonance in the slits of MNSAs; and (iii) all evanescent SP wave modes at the entrances/exits of slits, preventing direct diffraction of light into the semi-infinite dielectric or air.

In the numerical study [10], the metal of silver is used; on the top and bottom sides of the structures are a dielectric with refractive index of 1.47 and air. Inside the slits or microcavities is also air; the light sources are excited in TM polarization. The structures are defined by the dimensions of metal thickness (t), period (p), slit width (w) for both MNSAs and MC-MNSAs, and microcavity width (a) and height (b) in addition for MC-MNSAs, as indicated in Fig. 1(a). Figure 1(b) shows the transmission spectra of MC-MNSAs with different microcavity widths at $t=200$ nm, $w=80$ nm, $p=400$ nm, and $b=50$ nm. It is observed that the spectral lines are similar to that of a conventional MNSA [4,9]. But with an increase of the microcavity width, the peak position of the passband has a monotonous redshift in a wide spectrum range. Figures 1(c) and 1(d) show dependences of the passband peak on the microcavity width a and height b. Both are nearly linear in the near-IR (NIR) range. Slopes of the curves are obtained to be $\Delta\lambda_{peak}/\Delta a \sim 3.25$ for $b=100$ nm and 2.9 for $b=50$ nm in Fig. 1(c)

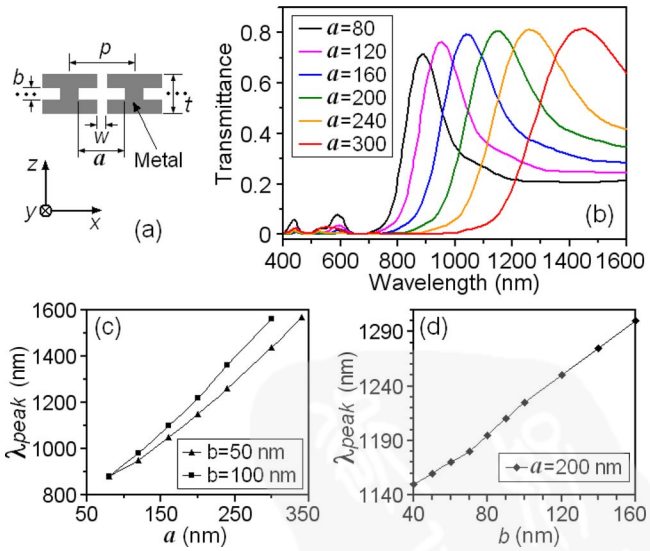

Fig. 1. (Color online) (a) Schematic illustration of an MC-MNSA. (b) Calculated transmission spectra of MC-MNSAs with different cavity widths a (in nanometers) at $t=200$ nm, $w=80$ nm, $p=400$ nm, and $b=50$ nm. (c) and (d) show dependences of the main transmission peak (λ_{peak}) on the cavity width a and height b, in which $t=200$ nm, $w=80$ nm, and $p=400$ nm.

0146-9592/09/091411-3/$15.00

and $\Delta\lambda_{peak}/\Delta b \sim 1.27$ for $a=200$ nm in Fig. 1(d). Because the peak wavelength is more dependent on the microcavity width, and also lateral (i.e., in-plane), variation of the structure dimensions in a thinner metal layer is technically more feasible with planar processing technologies; the microcavity width can be the primary factor for passband tuning of an MC-MNSA filter array.

Figure 2 shows the transmission spectra of MC-MNSAs with different periods, along with those of MNSAs for comparison. The transmission spectrum of a corresponding single slit or a single slit with an embedded microcavity in a continuous metal film is also shown in each plot (the values are normalized to scale in the plots). It is observed that, both for MNSAs in Fig. 2(a) and MC-MNSAs in Fig. 2(b), the main passband peaks do not simply show monotonous redshifting with increase of period but are split for larger periods and decrease in transmittance values. Meanwhile, all the main passbands are included within a "package" of the spectrum line of the single slit [in Fig. 2(a)] or single slit with an embedded microcavity [in Fig. 2(b)]. This phenomenon was explained by us for MNSAs [9]: The transmission spectra of periodic narrow slit arrays are resulted from superposition of transmission dips, induced by in-plane SP resonances, on the transmission spectra of individual slits, whose passbands are due to enhanced transmission by cavity resonances in the slits.

Note that the transmission of a single slit with or without an embedded microcavity in a continuous metal film is different from that in a periodically arrayed slit structure, which will be shown later. In addition, the in-plane SP resonances should be determined by the Bloch wave band-edge conditions for the in-plane propagating SP waves rather than the grating-assisted phase-matching conditions [9]; the latter just enhances excitation of in-plane SP waves. Therefore, the transmission dips are at the vacuum wavelengths of $\lambda_0=(2p/n)\sqrt{\varepsilon_m\varepsilon_d/(\varepsilon_m+\varepsilon_d)}$ ($n=1,2,\ldots$), which correspond to the band edges of in-plane SP Bloch waves. Here ε_m and ε_d are permittivities of the metal and dielectric (or air), and p is the structure period. Usually, the $n=1$ mode accounts for a spectrum dip on the longer-wavelength side of the main passband [9], and the higher-order ($n=2,3,\ldots$) modes result in spectrum dips on the shorter-wavelength side of the main passband [3,4,9]. But, with an increase of the period, the transmission dip of a higher-order resonance (usually for $n=2$) may shift into the passband of individual slits/microcavities and result in a splitting of the passband. Meanwhile, the transmittance of splitted peaks is decreased owing to a spread of the shift in resonance.

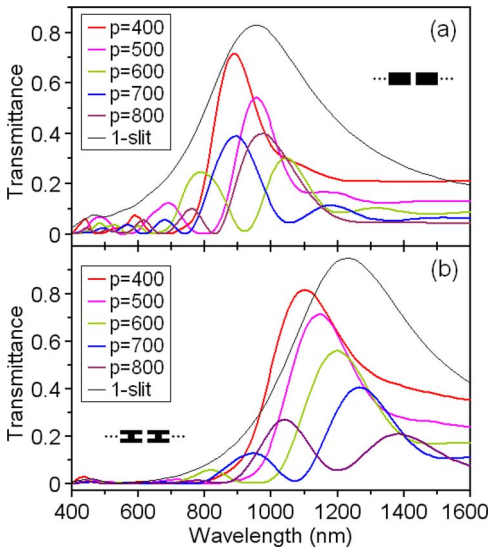

Fig. 2. (Color online) Calculated transmission spectra of (a) conventional MNSAs and (b) MC-MNSAs with different periods p (in nanometers), in which $t=200$ nm, $w=80$ nm for both, and $a=160$ nm, $b=50$ nm for (b). Transmission spectrum (relative values, normalized arbitrarily) of a corresponding single slit [in (a)] or single slit with an embedded microcavity [in (b)] in a continuous metal film (labeled "1-slit") is also shown for comparison.

Figure 3 shows the mode profile of a microcavity in an MC-MNSA. The cavity mode was excited with an impulse source in the microcavity, and a monitor in it recorded the maximum cavity intensity [11] at the vacuum wavelength of 1070 nm, which is considered to be the resonance wavelength of the microcavity in the MC-MNSA. This wavelength is nearly equal to the peak wavelength of the passband of the corresponding MC-MNSA ($p=400$ nm) in Fig. 2(b). It is observed in Fig. 3(b) that, by introducing a microcavity with enlarged width ($a>w$), the cavity mode becomes an optical mode, resonant in the transverse (x) direction. We know that, for MNSAs, it is an SP mode confined in slits, resonant only in the longitudinal (z) direction. Thus the MC-MNSA structure provides another dimension to tune the channeling resonances. Meanwhile, the field in the longitudinal direction of the slit (with microcavity) can still be as well confined as that of a MNSA, as shown in Fig. 3(c).

Figure 4 shows the calculated spectra of the cavity intensity inside single slits or microcavities of conventional MNSAs and MC-MNSAs with different periods, along with the spectra of corresponding single slits or microcavities in continuous metal films. Here, the cavity intensities are also normalized into scales of display and comparison. Same as in Fig. 3, an im-

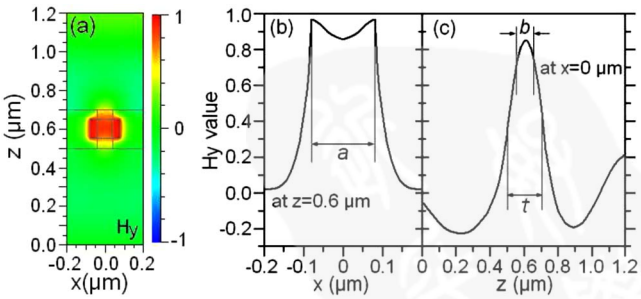

Fig. 3. (Color online) Calculated mode profile (H_y field distribution) of a microcavity in an MC-MNSA with $t=200$ nm, $w=80$ nm, $p=400$ nm, $a=160$ nm, and $b=100$ nm. (b) and (c) show the field values along the line of $z=0.6$ μm and the line of $x=0$ μm in the contour map (a).

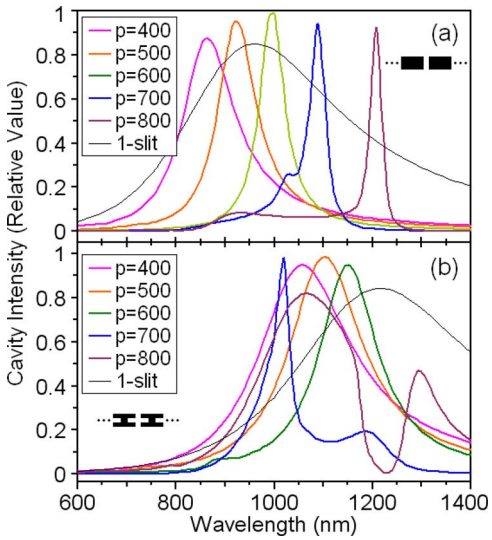

Fig. 4. (Color online) Calculated spectra of cavity intensity inside single slits or microcavities of (a) conventional MNSAs and (b) MC-MNSAs with different periods p (in nanometers), in which $t=200$ nm, $w=80$ nm for both, and $a=160$ nm, $b=100$ nm for (b). Spectra of cavity intensity for corresponding single slits or microcavities in continuous metal films (labeled "1-slit") are also shown in both plots.

pulse excitation source and a field monitor are set in a single slit or microcavity of an arrayed structure (MNSA or MC-MNSA) or a continuous metal film (for 1-slit cases). In investigation, it is found that the resonance of a single slit in a conventional MNSA or a microcavity in an MC-MNSA is different from that of a slit or microcavity of same dimensions in a continuous metal film. The difference is obviously due to the interaction between neighboring slits or microcavities in the arrayed structures. The interaction results in two main effects: (i) leakage of energy from the slit/microcavity excites in-plane SP waves at the top and bottom metal/dielectric (air) interfaces, which can also be resonant under Bloch wave band-edge conditions; and (ii) interaction between the neighboring slits/microcavities modifies the intrinsic cavity mode of individual slits/microcavities (1-slit case) and forms a period-dependent coupled-resonance mode of the arrayed slits/microcavities. These two effects can be observed in Figs. 4(a) and 4(b). Note that, although the effect (i) is not clear in the shorter wavelength range, it is very obvious when the plots are locally magnified. As shown in the plots, with an increase of period, the resonance peak initially has a monotonous redshift, but the trend is frustrated for the MNSAs and MC-MNSAs with larger periods (e.g., $p=700$ and 800 nm), for which the resonance bands become split. The band splitting is also related to the shift of the leakage-induced in-plane SP resonance into the cavity-resonance band of the slit/microcavity for larger periods. Particularly, the proximity of the resonance conditions of these two modes enhances the effect via their mode coupling. This explanation can be verified with simple calculations of the in-plane SP resonance positions or comparison with their counterparts in Figs. 2(a) and 2(b). As such, interference between the cavity mode and the in-plane resonance mode prevents one to design a filter array that can be monotonously tuned with variance of period in different segments. But it is found that, as the in-plane SP resonance is far away from the cavity resonance position (e.g., for smaller period $p=400$ nm), interference between the two modes disappears. Thus the peak position of cavity resonance in individual slits (of an MNSA) or microcavities (of an MC-MNSA) becomes nearly equal to the peak position of the main transmission passband of the MNSA or MC-MNSA, which can be confirmed by comparing Figs. 2 and 4 for $p=400$ nm.

From the above analysis, it can be seen that the MC-MNSA structure has potential applications for tunable filter arrays. Different segments of an array can be designed to have embedded microcavities with different cavity widths to tune the passbands of transmitted light.

This work has been supported by National Science Foundation of China (NSFC) (60707012), The Research Fund for the Doctoral Program of Higher Education (20070384022), the Science and Technology Key Project of Fujian Province of China (2007H0032), and the China-Ministry of Science and Technology International Science and Technology Cooperation and Exchange Project (008DFA51230).

References and Notes

1. U. Schröter and D. Heitmann, Phys. Rev. B **58**, 15419 (1998).
2. J. A. Porto, F. J. Garcia-Vidal, and J. B. Pendry, Phys. Rev. Lett. **83**, 2845 (1999).
3. Q. Cao and P. Lalanne, Phys. Rev. Lett. **88**, 057403 (2002).
4. Z. Sun, Y. S. Jung, and H. K. Kim, Appl. Phys. Lett. **83**, 3021 (2003).
5. Y. Xie, A. Zakharian, J. V. Moloney, and M. Mansuripur, Opt. Express **13**, 4485 (2005).
6. O. T. A. Janssen, H. P. Urbach, and G. W. 't Hooft, Opt. Express **14**, 11823 (2006).
7. D. J. Park, K. G. Lee, H. W. Kihm, Y. M. Byun, D. S. Kim, C. Ropers, C. Lienau, J. H. Kang, and Q-Han Park, Appl. Phys. Lett. **93**, 073109-1 (2008).
8. H. Kim, Z. Sun, and Y. S. Jung, U. S. patent 7,420,156 (September 2, 2008).
9. Z. Sun and D. Zeng, J. Mod. Opt. **55**, 1639 (2008).
10. The numerical calculations were performed with the software FullWAVE™ (ver. 6.0, RSoft Design Group, Inc.), which is based on the finite-difference time-domain method. In simulations, the periodic boundary conditions were applied in the periodic direction (x direction), and perfect-matching layer boundary conditions were applied in nonperiodic directions (x and/or z direction). Permittivity of silver is defined in the software as a sum of Lorenzian functions: $\varepsilon(\omega)=\varepsilon_\infty+\Sigma_k\Delta\varepsilon_k/[a_k(i\omega)^2-b_k(i\omega)+c_k]$, where ε_∞ is the value of permittivity in the limit of infinite frequency ω (unit, rad/μm), $\Delta\varepsilon_k$ is the strength of each resonance, and a_k, b_k, and c_k are fitting coefficients.
11. The cavity intensity is calculated as the field intensity $|H_y|^2$ integrated over the area of the monitor located in the cavity.